Check for updates

Decreasing Groundwater Supply Can Exacerbate Lake Warming and Trigger Algal Blooms

Ammar Safaie[1], Elena Litchman[2, 3], and Mantha S. Phanikumar[1*]

[1]Department of Civil and Environmental Engineering, Michigan State University, East Lansing, Michigan 48824, United States.
[2]Kellogg Biological Station, Michigan State University, Hickory Corners, Michigan 49060, United States.
[3]Department of Integrative Biology, Michigan State University, East Lansing, Michigan 48824, United States.
*Corresponding author: Mantha S. Phanikumar (phani@egr.msu.edu)
ORCID: https://orcid.org/0000-0001-9206-3129

Ammar Safaie ORCID: https://orcid.org/0000-0003-3327-2224
Elena Litchman ORCID: https://orcid.org/0000-0001-7736-6332

Key Points:

- Groundwater plays a significant role in key biophysical processes in an inland lake
- Deep waters in the lake can resist changes induced by surface warming
- Decreasing groundwater supply to inland lakes could cause deep water warming and trigger algal blooms

This article has been accepted for publication and undergone full peer review but has not been through the copyediting, typesetting, pagination and proofreading process, which may lead to differences between this version and the Version of Record. Please cite this article as doi: 10.1029/2021JG006455.

This article is protected by copyright. All rights reserved.

Accepted Article

Accepted Article

Abstract

As groundwater depletion becomes a global phenomenon, inland lake ecosystems are being impacted by decreasing groundwater supply. While the current trend of rapid surface warming of inland lakes continues, the deep waters can resist changes, depending on the nature of surface water – groundwater interactions. However, the effects of these interactions on lake processes are not fully understood. Here we investigate the role of groundwater on coupled biophysical processes in a deep, dimictic, groundwater-fed lake using mechanistic models combined with data from field observations. Although excess nutrient inputs are the most commonly cited reason for algal blooms, here we show that algal blooms in inland lakes can also appear due to a decreasing groundwater supply while all other factors remain the same. Results indicate that decreasing groundwater supply to lakes leads to elevated hypolimnetic temperatures, enhanced algal growth rates and algal blooms, and oxygen depletion, thus exacerbating the negative effects of surface warming. Our work suggests that globally declining groundwater supplies may have a significant negative effect on water quality of inland lakes by accelerating water column warming and stimulating algal growth, especially when the groundwater contribution to the lake system is significant compared to riverine discharge. The work provides insights for management efforts to improve the resilience of groundwater-dependent ecosystems in the face of external stressors.

Plain Language Summary

Harmful algal blooms in inland lakes and reservoirs contribute to significant economic losses annually while posing a range of health risks; however, the exact causes for the blooms are not always known. Using mechanistic models and field data, we reveal a link between groundwater supply and algal blooms in an inland lake. While previous research has demonstrated that excess nutrient inputs via both surface and subsurface discharges cause algal blooms, our work shows that decreasing groundwater supply alone could trigger algal

This article is protected by copyright. All rights reserved.

blooms in inland lakes by exacerbating lake warming while all other factors remain the same. Our results have implications for management efforts to mitigate the current trends of lake surface warming and declining groundwater levels in major aquifers throughout the world.

1 Introduction

Surface temperatures of inland lakes are on the rise across many regions around the globe in response to climate change (Magnuson, 2000; Piccolroaz et al., 2020; Schneider & Hook, 2010; Sharma et al., 2015; Woolway et al., 2020; Woolway & Maberly, 2020). The physical consequences of increasing lake surface temperatures and decreasing ice cover duration include changes in evaporation rates, mixing-regime, and increasing duration or intensity of thermal stratification (Sharma et al., 2019; Wang, 2018; Woolway et al., 2020). Moreover, seasonal changes in the timing and duration of overturn and stratification in response to climate change, link trends of surface warming to deep water temperatures of lakes (Anderson et al., 2021). These physical changes, in turn, alter the ecological functioning of lakes, nutrient cycling (Tong et al., 2021), oxygen availability (Zhang et al., 2015), primary production (O'Reilly et al., 2003; Verburg, 2003), and aquatic food web structure (Tanentzap et al., 2020). Temperature changes can alter the rates of chemical reactions, aquatic ecosystem metabolism, biological growth rates, photosynthesis and respiration rates and can disturb ecosystem equilibrium (Carpenter et al., 2011; Woolway et al., 2016). Moreover, increased water temperature and the subsequent changes in stratification often negatively affect water quality of inland water bodies (Chang et al., 2015). In addition, lake warming is associated with an increased risk of algal blooms, including toxic cyanobacteria, and eutrophication (Zhang et al., 2015), which can lead to oxygen depletion, more frequent periods of hypolimnetic hypoxia to anoxia that can amplify algal blooms further (Goto et al., 2012; Umaña, 2014; Zhang et al., 2016). However, lake responses to rising temperatures depend on geographic location, morphometry, mixing regime and trophic state (Kraemer et

This article is protected by copyright. All rights reserved.

Accepted Article

al., 2017; O'Reilly et al., 2015; Woolway et al., 2020). Three decades of satellite imagery data for 71 large lakes around the word indicated that while the intensity of algal blooms has increased in most of the lakes (68 percent), only the lakes that warmed less compared to other lakes had a reduced summertime bloom intensity (Ho et al., 2019).

Most previous studies have focused on global analysis of lake surface temperature trends to investigate the response of lakes to climate-induced changes (Maberly et al., 2020; Piccolroaz et al., 2020; Schneider & Hook, 2010; Sharma et al., 2015; Woolway et al., 2020). Despite the reported high correlation between rising air temperature and surface water temperature, the deepest parts of lakes demonstrate a higher persistence of lake temperature anomalies with inconsistent direction and magnitude of trends across individual lakes (Pilla et al., 2020; Woolway & Merchant, 2018). The warming signal in deeper waters of some small lakes gets damped, which suggests that there are other factors that control deep-water temperature, in addition to the meteorological drivers of surface water temperature trends (Pilla et al., 2020; Winslow et al., 2015). Some of those factors include decreases in water transparency (Pilla et al., 2018), feeding of cold water from glacial melt (Blais et al., 2001), and groundwater intrusion (Safaie et al., 2017a) but it is unknown how important they are. Hence, it is imperative to identify key external drivers and the impact of their changes to fully understand physical and ecological consequences of climate change on inland water bodies.

The responses of groundwater-fed lakes to climate-induced changes likely differ from those of other lakes, depending on the nature and strength of their interaction with groundwater. Shallow groundwater-fed lakes can have a significant bottom cooling in summer (Kettle et al., 2012), which may act as a self-regulating mechanism within a lake ecosystem and enhance the ability of the system to resist disturbances from surface-induced changes, such as warming. The rivers that are primarily groundwater-fed are buffered against increasing seasonal temperature variations (Qiu et al., 2019, 2020) as the incoming

This article is protected by copyright. All rights reserved.

Accepted Article

Accepted Article

groundwater flow at relatively lower temperatures holds more oxygen to support aquatic organisms (Combes, 2003). In fact, groundwater serves as a buffer against external changes keeping the system in a less altered state. On the other hand, changes in the magnitude of groundwater discharge to lakes can cause severe environmental impacts on groundwater-dependent ecosystems. Since the dynamics of algal growth depends on nutrient availability, nutrient-enriched groundwater discharging to the lake can have significant impact on nutrient-algal dynamics (Essaid et al., 2020; Shaw et al., 2017). Moreover, groundwater flow with contamination by sewage water to lakes is identified as the primary cause of coastal eutrophication (Timoshkin et al., 2018). Thus, it is crucial to understand the role of groundwater in biophysical processes and water quality of inland lakes.

Although groundwater-dependent ecosystems tend to show greater resilience to external stressors, maintaining the resilience of such ecosystems relies upon the sustainability of ground-water resources. Numerous studies indicate long-term groundwater depletion in many major aquifers across the world (Dalin et al., 2017; Gurdak, 2017; Rodell et al., 2009; Wada et al., 2010). Climatic and human-induced groundwater table drawdown could cause shifts in the physical, chemical, and biological structure of groundwater-fed lakes (Gurrieri & Furniss, 2004; Turner & Townley, 2006; Webster et al., 1996) but the effects of such drawdowns remain unexplored. Therefore, with groundwater levels decreasing in many parts of the world, there is an urgent need to understand how lake ecosystems respond to the changing nature of groundwater - surface water interactions.

Here, we show that decreasing groundwater contributions to groundwater-fed inland lakes can cause deep water warming and stimulate algal blooms, thus negatively affecting water quality. By combining extensive field data and numerical modeling, we developed a coupled biophysical model of Gull Lake, a relatively deep inland lake in Michigan, USA. Gull Lake is a dimictic, groundwater-fed lake with strong summer stratification and with

This article is protected by copyright. All rights reserved.

Accepted Article

bottom cooling controlled by groundwater (Perry and Brown, 1942; Tague, 1977; Kinsman-Costello et al., 2015; Safaie et al., 2017a). A detailed three-dimensional hydrodynamic model of the lake-groundwater system was developed to simulate lake circulation and thermal structure and tested using field observations (Safaie et al., 2017a). In the present work, the hydrodynamic model was coupled with transport models to evaluate the role of groundwater on hypolimnetic temperatures, dissolved oxygen, nutrients, and algal dynamics within the lake. The developed model was used to predict changes in the lake ecosystem caused under two scenarios of groundwater depletion: 1) with half of the groundwater contribution relative to current conditions and 2) in the absence of groundwater contribution. These scenarios were defined based on observations reported in previous studies. For example, estimation of groundwater storage change based on *in situ* and remotely sensed groundwater data in the Lake Chad Basin indicated that the groundwater water storage could decrease to half of its value and even to zero due to both climate change and overexploitation of water (Skaskevych et al., 2020).

2 Materials and Methods

2.1 Site Description

Gull Lake is a relatively deep (33.8 m maximum depth, and 12.5 m average depth) and large (8.25 km^2 surface area) glacial kettle lake located in south- western Michigan, USA. Gull Lake is a hardwater, groundwater-fed lake, which is one of the most common types of lakes in Michigan. The total alkalinity of the lake is reported as 3 meq L^{-1}, Phosphorus (P) limits phytoplankton growth (total P around 9 μg P L^{-1}), and the lake is oligotrophic to mesotrophic (Bruesewitz et al., 2012). Gull Lake receives water from three small lakes (Little Long, Wintergreen and Miller Lakes), but its main surface inflow is from Prairieville Creek with an average flow rate of 0.19 m^3/s in 2015. There is also an outflow at the south of the

This article is protected by copyright. All rights reserved.

lake (Figure 1). The average groundwater inflow and outflow were estimated as 0.77 and 0.40 m^3/s respectively in 2015 (Safaie et al., 2017a). Given the contribution of groundwater to the lake water balance (about 50% of total water inputs), the water residence time of the lake is equal to 2.52 yr (Safaie et al., 2017a). Moreover, a strong stratification is developed in summer due to the bottom cooling controlled by groundwater. The presence of the cool deep waters isolated from epilimnion makes the lake a suitable habitat for both warm- and cold-water fish species.

2.2 Field sampling and laboratory analyses

Vertical profiles of water quality parameters of Gull Lake, MI were regularly collected weekly at the deepest part of the lake (Figure 1) during the summer between 2008 and 2017. In addition, semidiurnal intensive *in situ* measurements were carried out around 10:00 AM and 2:00 PM for two weeks in August of 2015. Depth-integrated samples of the surface water were collected by a four-meter integrated sampler. Moreover, water samples were collected at the surface, the depth of deep chlorophyll maxima (DCM), and the bottom of the lake. Positions of DCM were estimated based on the depth of the maximum *in situ* fluorescence which were measured during each filed work by a Self-Contained Autonomous Micro-Profiler (SCAMP, http://pme.com). Nutrient analyses of water samples were performed to measure total phosphorus, dissolved inorganic phosphorus, total nitrogen, dissolved nitrate, and chlorophyll concentrations. Additionally, a Hydrolab multi-parameter sonde was utilized to measure vertical profiles of temperature, dissolved oxygen (DO), and chlorophyll concentration in the water column with 0.5- 1 m depth intervals. Measurements of DO were done based on a luminescent-based optical sensor (ASTM D888, 2012). Nitrogen analyses were conducted using second-derivative spectroscopy (Crumpton et al., 1992). Second-derivative UV spectroscopy for filtered samples was used for nitrate determination. Total N was calculated based on second derivative analyses of nitrate after the persulfate

This article is protected by copyright. All rights reserved.

Accepted Article

digestion of unfiltered samples. A Lachat Quickchem autoanalyzer was used to analyze filtered samples for measurement of dissolved inorganic phosphorus (orthophosphate or soluble reactive phosphorus, SRP). Unfiltered samples were digested by the persulfate digestion method to determine total P.

2.3 Biophysical model of Gull Lake

A fully coupled biophysical model of Gull Lake was developed based on three-dimensional, unstructured grid, Finite-Volume Community Ocean Model (FVCOM) (Chen et al., 2003, 2006). The governing hydrodynamic equations of FVCOM, including continuity, momentum, temperature, salinity, and density equations were closed with a two-equation $k-\varepsilon$ turbulence model (Rodi, 1987) and Smagorinsky turbulent closure (Smagorinsky, 1963) schemes for vertical and horizontal mixing, respectively. To do this, FVCOM was coupled to General Ocean Turbulent Model (GOTM, http://www.gotm.net) (Burchard et al., 1998). An unstructured mesh in the horizontal plane was constructed with 20,604 nodes and 40,260 triangular elements. The Gull Lake-FVCOM model was configured with horizontal grid resolutions ranging from 5 m near the shoreline to 75 m in the offshore regions of the lake. A terrain- following sigma vertical coordinate system was used with 30 σ-layers. The bathymetry of the lake was collected using a SonTek RiverSurveyor M9 system and interpolated over the mesh using the natural neighbor method (Safaie et al., 2017b). Hourly meteorological data were obtained from land-based weather stations around the lake to construct the meteorological forcing for the hydrodynamic model. Details of meteorological data besides the hydrodynamic model of the lake - groundwater system and its validation against *in situ* observations can be found in Safaie et al. (2017a). To assess the performance of the model in simulating lake - groundwater interactions including water exchange fluxes, we used high-resolution Acoustic Doppler Current Profiler observations of currents, vertical

This article is protected by copyright. All rights reserved.

Accepted Article

profiles of water temperature from thermistor chains and lake levels in our previous study (Safaie et al., 2017a).

The water quality model with inclusion of the benthic fluxes was developed based on the EPA Water quality Analysis Simulation Program (WASP5) (Ambrose et al., 1993). The water quality model, which was coupled with FVCOM (FVCOM-WQM), simulated nutrient cycling, dissolved oxygen budget, and phytoplankton biomass. Observed nutrient concentrations in Prairieville Creek and the water supply well at the Pond Laboratory at Kellogg Biological Station (Table 1) were obtained from KBS-LTER database (https://lter.kbs.msu.edu/datatables) and used to define riverine and benthic fluxes of nutrients. The water quality model was first calibrated based on semidiurnal intensive *in situ* measurements through the water column conducted for two weeks in August of 2015 at the deepest part of the lake. Then, the performance of the model was evaluated using the weekly measurements of vertical profiles of water quality variables. Once the model parameters were calibrated based on the intensive measurements, we ran the model using the same parameters for the whole simulation period and evaluated the performance of the model based on the weekly data collected in 2014 and 2015.

To systematically quantify the biophysical responses of the lake to decreasing groundwater contribution, the developed model was run under three scenarios. First, the model was implemented to simulate existing conditions reflecting the current contribution of groundwater to the lake (scenario 1). Next, the model was run with half of the current groundwater contribution (scenario 2). Temperature and nutrient fluxes changed automatically proportional to the reduction in the groundwater flux. Finally, the lake dynamics was simulated in the absence of any groundwater input to the lake (scenario 3).

This article is protected by copyright. All rights reserved.

Accepted Article

Accepted Article

The governing equations describing the concentrations of dissolved oxygen, biochemical oxygen demand, algae, phosphorus, and nitrogen species are as follows. The general mass balance equation for the water quality components can be written as:

$$\frac{\partial C_i}{\partial t} + \frac{\partial (uC_i)}{\partial x} + \frac{\partial (vC_i)}{\partial y} + \frac{\partial (wC_i)}{\partial z} = \frac{\partial}{\partial x}(A_h \frac{\partial C_i}{\partial x}) + \frac{\partial}{\partial y}(A_h \frac{\partial C_i}{\partial y}) + \frac{\partial}{\partial z}(K_h \frac{\partial C_i}{\partial z}) + S_i \quad (1)$$

where $C_i (i = 1,...,8)$ are the concentrations of the eight water quality state variables, including Dissolved Oxygen (DO) (mg O_2/L), Carbonaceous Biochemical Oxygen Demand (CBOD) (mg C/L), phytoplankton (mg C/L), NH_3 (mg N/L), NO_3 (mg N/L), ON (mg N/L), OPO_4 (mg P/L), and OP (mg P/L), respectively. OPO_4 was measured in μg/L. Since all units in FVCOM were in mg/L, the units of OPO_4 in the model input and output were converted accordingly. u, v, w are velocity components in the x, y, z directions; A_h and K_h denote the horizontal and vertical mixing coefficients respectively; $S_i (i = 1,...,8)$ denote the internal source/sink terms. Since advection and dispersion terms are the same for all transport equations, the source/sink terms are described in more detail below.

Dissolved oxygen (C_1). The dynamics of dissolved oxygen are controlled by the following processes (Ambrose et al., 1993): reaeration, oxidation, nitrification, phytoplankton loss, phytoplankton growth, sediment oxygen demand, and bacterial respiration. The term that includes all these processes can be written as follows:

$$S_1 = k_{reae} q_{reae}^{(T-20)} (C_S - C_1) - k_{deox} q_{deox}^{(T-20)} \frac{C_1 C_2}{K_{BOD} + C_1} - \frac{64}{14} k_{nitr} q_{nitr}^{(T-20)} \frac{C_1 C_4}{K_{nitr} + C_1} - \frac{32}{12} D_P C_3 + G_P \left[\frac{32}{12} + \frac{48}{14} a_{nc} (1 - P_{NH_3}) C_3\right] - \frac{SOD}{h_b} q_{SOD}^{(T-20)} - k_{bresp} \quad (2)$$

This article is protected by copyright. All rights reserved.

The first term in equation (2) is the reaeration term, where k_{reae} is the reaeration rate coefficient at 20 ℃ (day^{-1}) and q_{reae} is the temperature coefficient of reaeration. C_S and C_1 denote the dissolved oxygen saturation and dissolved oxygen concertation (mg O_2/L), respectively. C_S which is a function of temperature and salinity is given by (APHA, 1998):

$$\ln C_S = -139.34411 + \frac{1.575701 \times 10^5}{T_K} - \frac{6.642308 \times 10^7}{T_K^2} + \frac{1.243800 \times 10^{10}}{T_K^3} - \frac{8.621949 \times 10^{11}}{T_K^4} - 0.5535 \times S\left(0.031929 - \frac{19.428}{T_K} + \frac{3867.3}{T_K^2}\right) \quad (3)$$

where T_K is the water temperature in Kelvin (K). k_{reae} in the first term of equation (2) is calculated as the maximum of wind-induced and flow-induced reaeration. Oxygen reaeration induced by wind is obtained using the method described in O'Connor (1983). Flow-induced reaeration is determined as a power function of average hydraulic depth and velocity using the Covar formulation (Covar, 1976).

The second term of equation (2) is the CBOD oxidation, where k_{deox} is the CBOD deoxygenation rate at 20 ^oC (day^{-1}) and q_{reae} is the temperature coefficient of deoxygenation. C_2 and K_{BOD} denote CBOD concentration and the half-saturation constant for oxygen limitation of CBOD oxidation (mg O_2/L), respectively. The third term of equation (2) represents nitrification, where k_{nitr} is the nitrification rate at 20 ℃ (day^{-1}) and q_{nitr} is the temperature coefficient of nitrification. C_4 and K_{nitr} are concentration of NH_3 and the half-saturation constant for oxygen limitation of nitrification (mg O_2/L), respectively. The fourth term in equation (2) shows phytoplankton oxygen consumption due to its respiration and death, where D_P is the phytoplankton loss (day^{-1}), and C_3 is the concentration of phytoplankton (mg C/L).

The fifth term in equation (2) denotes oxygen production by phytoplankton photosynthesis and nitrogen reduction, where G_P is the growth rate of phytoplankton (day^{-1}),

This article is protected by copyright. All rights reserved.

Accepted Article

a_{nc} is the stoichiometric ratio of nitrogen to carbon in phytoplankton. Dissolved inorganic nitrogen is taken up by for phytoplankton growth. Both ammonia and nitrate can be consumed by phytoplankton. However, ammonia nitrogen is the preferred form, so the ammonia preference term was used to model their ammonia preference (Ambrose et al., 1993):

$$P_{NH_3} = \frac{C_4 C_5}{(C_4 + 0.0001K_{mN})(C_5 + 0.0001K_{mN})} + \frac{0.0001C_4 K_{mN}}{(C_4 + C_5)(C_5 + 0.0001K_{mN})} \quad (4)$$

The last two terms of equation (2) are the sediment oxygen demand (SOD) and the oxygen consumption by bacterial respiration, respectively, where h_b is the benthic layer depth (m), q_{SOD} is the temperature coefficient of SOD, is the sediment k_{bresp} is the bacterial respiration rate (mg O_2/day).

At the bottom of the lake, the following equation was solved to model the *DO* flux from the benthic layer to the water column:

$$\left.\frac{\partial C_1}{\partial t}\right|_{z=-H} = D_z \frac{\partial^2 C_1}{\partial z^2} \quad (5)$$

where D_z denotes diffusive exchange coefficient (m^2/day).

Carbonaceous biochemical oxygen demand (C_2). The amount of Carbonaceous Biochemical Oxygen Demand (CBOD) in a water body depends on phytoplankton loss, oxidation, denitrification, and settling, which can be described by the following equation:

$$S_2 = \frac{32}{12} D_P C_3 - k_{deox} q_{deox}^{(T-20)} \frac{C_1 C_2}{K_{BOD} + C_1} - \frac{5}{4}\frac{32}{14} k_{deni} q_{deni}^{(T-20)} \frac{K_{NO_3} C_5}{K_{NO_3} + C_1} - (1 - f_{D2}) v_{S2} \frac{\partial C_2}{\partial z} \quad (6)$$

This article is protected by copyright. All rights reserved.

where K_{NO_3} = half-saturation concentration for oxygen limitation of denitrification (mg O_2/L), f_{D2} = fraction of dissolved CBOD, C_s is the dissolved oxygen saturation (mg O_2/L) estimated by equation (3), and v_{s2} =organic matter settling velocity (m.day^{-1}).

Phytoplankton (C_3). Sources and sinks of phytoplankton are mainly described by the following processes: phytoplankton growth, phytoplankton loss, and phytoplankton settling:

$$S_3 = G_P C_3 - D_P C_3 - v_{S3} \frac{\partial C_3}{\partial z} \tag{7}$$

where v_{s2} = phytoplankton settling velocity (m.day^{-1}), and the remaining variables have the same definition as those in equation (2). The growth rate of phytoplankton (G_P) is modeled as:

$$G_P = k_{grow} R_N R_I q_{grow}^{(T-20)} \tag{8}$$

where k_{grow} is the optimum phytoplankton growth rate at 20 ^oC (day^{-1}), R_N is the growth rate reduction due to nutrient limitation, R_I denotes growth rate reduction due to light limitation, and q_{grow} is the temperature coefficient of optimum growth. R_N is determined using the Michaelis-Menten model for inorganic nutrients:

$$R_N = \min\left[\frac{C_4 + C_5}{K_{MN} + C_4 + C_5}, \frac{C_7}{K_{MP} + C_7}\right] \tag{9}$$

where K_{MN} and K_{MP} are half-saturation constants for uptake of inorganic nitrogen (mg N/L) and phosphorus (mg P/L), respectively. R_I is determined using the model proposed by (Steele, 1962), which has the following form:

$$R_I = \frac{I_z}{I_s} \exp\left[1 - \frac{I_z}{I_s}\right] \tag{10}$$

This article is protected by copyright. All rights reserved.

where I_s is the optimum light intensity (W/m^2), and I_z is the light intensity in a water column. I_z is an exponential function of water depth that can be calculated using Beer's law:

$$I_z = I_0 \exp(-k_e z) \tag{11}$$

where I_0 is the light intensity at the surface (W/m^2), z is the water depth (m). k_e denotes the light extinction coefficient (m^{-1}) which can be calculated as the sum of the vertical light attenuation coefficient for pure water (k_w) and the phytoplankton self-shading attenuation (k_{shd}). Light intensity attenuates by the presence of phytoplankton biomass in a column of water. Self-shading of light by algae growing in a column of water can be expressed as (Ambrose et al., 1993):

$$k_{shd} = 0.0088Chl + 0.054Chl^{0.667} \tag{12}$$

where Chl is the chlorophyll concentration (μg/L) at water depth z. Chlorophyll concentrations can be estimated by $Chl = C_2 / a_{cchl}$, where a_{cchl} is the ratio of carbon to chlorophyll. Substitution of equation (11) into equation (10) in a layer-integrated form is used to calculate R_I:

$$R_I = \frac{2.718}{(k_e \Delta z)} \left\{ \exp\left[-\frac{I_0}{I_s} \exp(-k_e z_{i+1}) \right] - \exp\left[-\frac{I_0}{I_s} \exp(-k_e z_i) \right] \right\} \tag{13}$$

where z_i and z_{i+1} are depths from the free surface to the bottom and top of each sigma layer (m), respectively, and Δz is the layer thickness (m).

The phytoplankton loss rate (D_P) used in equations (2) and (7) is determined by considering phytoplankton respiration and mortality:

$$D_P = k_{resp} q_{resp}^{(T-20)} + k_{mort} q_{mort}^{(T-20)} \tag{14}$$

This article is protected by copyright. All rights reserved.

where k_{resp} = phytoplankton respiration rate at 20 ^{o}C (day^{-1}); q_{resp} = temperature coefficient of phytoplankton respiration; k_{mort} = rate of phytoplankton mortality at 20 ^{o}C (day^{-1}); and q_{mort} = temperature coefficient of phytoplankton mortality.

Ammonia (C_4). Ammonia, NH_3, is obtained by the balance between phytoplankton loss, mineralization from organic nitrogen, phytoplankton uptake, and nitrification:

$$S_4 = a_{nc} D_P (1 - f_{ON}) C_3 + k_{mine1} q_{mine1}^{(T-20)} \frac{C_3 C_6}{K_{mPC} + C_3} - a_{nc} G_P P_{NH_3} C_3 - k_{nitr} q_{nitr}^{(T-20)} \frac{C_1 C_4}{K_{nitr} + C_1} \quad (15)$$

where a_{nc} = the stoichiometric ratio of nitrogen to carbon in phytoplankton; D_P = phytoplankton loss rate (day^{-1}); f_{ON} = fraction of dead and respired phytoplankton recycled to the organic nitrogen pool; k_{mine1} = organic nitrogen mineralization at 20 ^{o}C (day^{-1}); q_{mine1} = temperature coefficient of organic nitrogen mineralization; K_{mPC} = half-saturation constant of phytoplankton limitation of phosphorus recycle (mg C/L); G_P = phytoplankton growth rate (day^{-1}); P_{NH_3} = constant of ammonia preference; k_{nitr} = nitrification rate at 20 ℃ (day^{-1}); q_{nitr} = temperature coefficient of nitrification; and K_{nitr} = half-saturation constant for oxygen limitation of nitrification (mg O_2/L).

Nitrate and nitrite nitrogen (C_5). Nitrogen oxides, including NO_2 and NO_3, are inorganic compounds of nitrogen, which can be described via nitrification, phytoplankton uptake, and denitrification processes:

$$S_5 = k_{nitr} q_{nitr}^{(T-20)} \frac{C_1 C_4}{K_{nitr} + C_1} - a_{nc} G_P (1 - P_{NH_3}) C_3 - k_{deni} q_{deni}^{(T-20)} \frac{K_{NO_3} C_5}{K_{NO_3} + C_1} \quad (16)$$

where k_{denit} = denitrification rate at 20 ^{o}C (day^{-1}); q_{denit} = temperature coefficient of denitrification; K_{NO_3} = half-saturation constant for oxygen limitation of denitrification (mg

This article is protected by copyright. All rights reserved.

O_2/L); and the remaining variables have the same definition as those in equation (15). The first term of equation (16) represents the nitrification that ammonia (NH_3) is oxidized to nitrite (NO_2^-) and then to nitrate (NO_3^-). The second term shows the preferred amount of NO_3 that is consumed by phytoplankton via the photosynthetic process. The last term in equation (16) is the denitrification that corresponds to the reduction of nitrate to nitrogen gas (N_2).

Organic nitrogen (C_6). Sources and sinks for organic nitrogen (ON) are obtained by phytoplankton loss, organic nitrogen mineralization, and ON settling. These processes can be determined as:

$$S_6 = a_{nc} D_P f_{ON} C_3 - k_{mine1} q_{mine1}^{(T-20)} \frac{C_3 C_6}{K_{mPC} + C_3} - (1 - f_{D6}) v_{S6} \frac{\partial C_6}{\partial z} \qquad (17)$$

where f_{D6} = fraction of dissolved organic nitrogen, and v_{S6} = settling velocity of organic nitrogen (m.day^{-1}).

Inorganic phosphorus (C_7). The amount of inorganic phosphorus (Orthophosphorus), OPO_4, in a water body include phytoplankton loss, mineralization from organic phosphorus, and phytoplankton uptake. These processes are determined in the following form:

$$S_7 = a_{pc} D_P (1 - f_{OP}) C_3 + k_{mine2} q_{mine2}^{(T-20)} \frac{C_3 C_8}{K_{mPC} + C_3} - a_{pc} G_P C_3 \qquad (18)$$

where a_{pc} = the stoichiometric ratio of phosphorus to carbon in phytoplankton; f_{ON} = fraction of dead and respired phytoplankton recycled to the organic phosphorus pool; k_{mine2} = organic phosphorus mineralization at 20 ^{o}C (day^{-1}); q_{mine2} = temperature coefficient of organic phosphorus mineralization; K_{mPC} = half-saturation constant of phytoplankton limitation of phosphorus recycle (mg C/L).

This article is protected by copyright. All rights reserved.

Organic phosphorus (C_8). Sources and sinks for organic phosphorus (OP), in a water body depends on phytoplankton loss, OP mineralization, and OP settling velocity. These processes are described by the following equation:

$$S_8 = a_{pc} D_P f_{OP} C_3 - k_{mine2} q_{mine2}^{(T-20)} \frac{C_3 C_8}{K_{mPC} + C_3} - (1 - f_{D8}) v_{S8} \frac{\partial C_8}{\partial z} \quad (19)$$

where f_{D8} denotes fraction of organic phosphorus, and v_{S8} is the settling velocity of organic phosphorus (m day^{-1}). Further detailed descriptions of the water quality model are available in Zheng et al. (2004) and Safaie (2017).

To simulate nutrient and algal transport at the lakebed, a benthic layer was added to the bottom of the water column. The following equation was defined in the benthic layer (at $z = -H$) that received groundwater inflow:

$$\frac{\partial C_i}{\partial t} + q_{in} \frac{\partial C_i}{\partial z} = D_z \frac{\partial^2 C_i}{\partial z^2} \quad (20)$$

where q_{in} is the groundwater inflow rate (m s^{-1}), D_z the vertical diffusion coefficient (m^2 s^{-1}). Benthic discharge in the losing portion of the lake was described as:

$$\frac{\partial C_i}{\partial t} + q_{out} \frac{\partial C_i}{\partial z} = 0 \quad (21)$$

where q_{out} is rate of groundwater outflow (m s^{-1}). Values of groundwater fluxes and the vertical diffusion coefficient were set as reported in (Safaie et al., 2017a).

3 Results and discussion

Vertical profiles of water quality variables from weekly *in situ* measurements at the deepest (32 m) region of the lake (Figure 1) show several interesting features between 2008 and 2017. The lake has strong summer thermal stratification, and the thermocline is generally

This article is protected by copyright. All rights reserved.

Accepted Article

formed at depths from 8 to 12 m. Although there was a high correlation between air temperature and surface water temperature (Figure 2a) of Gull Lake ($r(n=300) = 0.80$, $p < 0.01$), the bottom water temperature remained relatively stable over time compared with interannual changes of air and lake surface water temperatures. The highest and lowest maximum observed water temperature differences between lake surface and lake bottom were 20 and 15 °C in 2013 and 2014, respectively. Weekly time series of surface water temperatures show an increasing trend, while lake bottom temperatures and chlorophyll *a* (chl *a*) concentrations show a decreasing trend over the 10-year period (Figure S1). While the annual average air temperature was on the rise (+ 0.045 °C year^{-1}), the annual average deep-water temperature had a decreasing trend (− 0.071 °C year^{-1}) which was in line with the decline of the annual average deep chlorophyll maximum (DCM) (− 0.181 μg C L^{-1}) between 2009 and 2017. The biomass of the annual average DCM in 2014 was the highest (3.20 μg C L^{-1}) over the 2009 - 2017 period. It should be noted that since these observations are based on summer measurements, the trend describes the increased isolation of hypolimnion likely because of delays in fall mixing that have taken place due to warming climate conditions. Following the recent findings in Lake Michigan (Anderson et al., 2021), this condition can be paired with deep-water warming trends in the winter if subsurface water temperature measurements are available throughout the year.

Values of the parameters used in the water quality model are summarized in Table 2. The model performance metrics, including the coefficient of determination (R^2) and the root-mean-square error (RMSE)are summarized in Table 3. Based on these metrics the simulated results (scenario 1) were in good agreement with the observations. In scenario 1 representing current conditions, the groundwater inflow constituted approximately 40 to 56 percent of the water budget of the lake (Safaie et al., 2017a). When groundwater contribution was halved in scenario 2 and eliminated in scenario 3, the simulated lake levels dropped by 21 cm and 30

This article is protected by copyright. All rights reserved.

Accepted Article

cm, respectively, within the four-month simulation period (from early May to mid-September). The predicted decline of the lake level in transition from a fully connected to a fully disconnected flow regime is expected to be greater, since a fully disconnected groundwater-lake system loses more water due to higher water infiltration rates (Brunner et al., 2009), a process not included in our modeling. Moreover, as shown in Figures 3 and 4, the hypolimnion water temperature, which had a narrow range of temperature variability around 8.2 ^{o}C, increased by 2 ^{o}C in scenario 2 and more drastically by 6 ^{o}C in scenario 3 at the end of the simulation due to the absence of groundwater. These changes in thermal structure can strongly influence the abundance and distribution of aquatic species and could potentially pose a threat to cold-water fish species (Comte et al., 2013).

Contour plots of chl *a* for the three scenarios in 2015 are shown in Figure 5. Near-surface chlorophyll concentrations (0-4 m) were relatively low and uniform with the average concentration of 1.08 μg C L^{-1} in scenarios 1 and 2. In scenario 3, however, the average near-surface chlorophyll concentrations increased to 5.22 μg C L^{-1} after day of the year (DOY) 230 (see Figure 5c). As shown in Figures 5b and 5c., the phytoplankton bloom intensity increased with decreasing groundwater contribution. Mean and maximum values of simulated chl *a* for all scenarios are presented in Table 4. The increase in temperature in the second and third scenarios caused the average chl *a* to increase about 2.1 times in 2015. In addition, the maximum values of simulated chl *a* in the second and third scenarios were 1.29 and 3.75 times greater than those observed in 2015, respectively. This increasing algal biomass changed the algal vertical distribution due to self-shading of light by algae growing in the water column (Shigesada & Okubo, 1981). Thus, the position of DCM moved upward to the surface in the water column (see Figures 5c and 6). For instance, in DOY 244, positions of DCM were 13, 10.7, and 9.5 m below the surface of the lake in scenarios 1-3, respectively. These changes also altered the vertical distributions of dissolved oxygen (DO) (Figures 7 and

This article is protected by copyright. All rights reserved.

Accepted Article

8) and nutrients (Figures S2 and S3). For instance, the depths of DCM and oxycline were reduced by 3 m in DOY 235 in 2015 (see Figures 5c and 7c). Based on the simulation results for the three scenarios and following the chlorophyll limits suggested by the Organization for Economic Cooperation and Development (OECD) (OECD, 1982), the trophic status of the lake would change in both 2014 and 2015 from oligotrophic to mesotrophic due to decreasing groundwater contribution. The average trophic state index (TSI) derived from chlorophyll (Carlson, 1977) increased from 28-32 to 38-41 (Table 4) with decreasing groundwater supply, which highlights deterioration of trophic state. Warming and eutrophication under the decreased groundwater supply scenario would lead not only to an increase of algal biomass but it could also preferentially stimulate cyanobacteria that cause harmful algal blooms (HABs), because cyanobacteria have higher temperature optima for growth (Xiao et al., 2019).

Excessive growth and photosynthesis of phytoplankton in turn highly impacted the DO distribution, and this was further exacerbated by groundwater depletion (Figures 7 and 8). While the predicted dissolved oxygen concentration above the thermocline reached supersaturation with DO saturations ranging between 120 and 200% (Figure 9), warmer bottom temperatures lead to early hypoxia and anoxia in the deep waters of the lake. This level of oxygen supersaturation might increase the risk of gas bubble disease, bacterial infection, and mortality in invertebrates and fish (Elston & Wood, 1983; Harris et al., 2005). In scenario 1, bottom DO had a depletion rate of approximately 0.22 mg O_2 L^{-1} day^{-1}, and the anoxia occurred within four weeks. In scenario 3, however, the anoxic conditions occurred 12 days earlier, with a depletion rate of 0.36 mg O_2 L^{-1} day^{-1} due to the absence of a counteracting groundwater effect. This result suggests that cold-water fish species could experience a high oxythermal stress due to the depletion of deepwater dissolved oxygen,

This article is protected by copyright. All rights reserved.

Accepted Article

along with the deepwater warming due to decreasing groundwater contribution (Jiang & Fang, 2016).

The simulated results of 2014 were also consistent with those described for 2015 (Figures S4-S12). At the end of the simulation, the lake bottom temperature increased form 9.4 in scenario 1 to 11.4, 14.8 ^{o}C in scenarios 2 and 3, respectively (Figures S4 and S5). The phytoplankton growth rate increased with increasing water temperature. As shown in Table 4, the mean chl *a* concentration increased from 2.25 μg C L^{-1} in scenario 1 to 2.99 and 4.33 μg C L^{-1} in scenarios 2 and 3, respectively. The maximum chl *a* concentrations also increased to 11.1 and 24.59 μg C L^{-1} in scenarios 2 and 3, respectively. While the position of DCM varied from 12 to 14 m below the surface in scenarios 1 and 2 (Figure S6), it moved upward towards the surface by more than 3 m in the third scenario. For example, DCM positions in scenarios 1-3 on DOY 238 in 2014 were 14, 13.0, and 10.7 m below the surface of the lake respectively (Figure S7). In addition, DO levels above the thermocline increased due to accelerated phytoplankton growth (Figures S8 and S9). On the other hand, the concentrations of nutrients, especially near the positions of the DCM, decreased in scenarios 2 and 3 in consequence to the elevated phytoplankton uptake (Figures S10 and S11). As groundwater supply decreased, the lake's warming, and enhanced algal growth rates altered the DO saturation distribution (Figure S12). For instance, DO saturation at 10.4 m water depth on DOY 243 in year 2014 increased from 80% in scenario 1 to 123% in scenarios 3.

4 Conclusions

In this study, coupled process-based models of lake - groundwater systems combined with high-resolution field measurements were used to investigate the role of groundwater on several biophysical processes in Gull Lake. The impact of groundwater reduction/loss is not included in the riverine inputs, because the river contribution to the water balance of the lake

This article is protected by copyright. All rights reserved.

Accepted Article

Accepted Article

is relatively small compared to the groundwater input. In other study areas where the river contribution is significant, this impact needs to be investigated as well. Furthermore, we ran all scenarios from the same initial conditions to highlight the significant role of groundwater on water quality in flow-through lakes such as the Gull Lake. In future work, there is a need to study the long-term effects of groundwater on thermal structure and water quality of the lake. To improve our understanding of seasonal changes in the thermal structure of lakes such as the Gull Lake, year-round observations are necessary. Our work shows that algal blooms can appear as a response of inland lakes to decreasing groundwater supply and indicates that there is significant bottom cooling during the summer months caused by groundwater-lake interactions, which play an important role in water quality, biodiversity, and habitat structure of the lakes. Decreasing groundwater supply can reduce the ability of inland lakes to buffer seasonal water temperature variations leading to an increase in water temperatures and changes in the thermal structure of the lakes. Consequently, the ecological function of lakes, including nutrient cycling, dissolved oxygen stratification, and algal dynamics are impacted. Additionally, groundwater depletion could alter food-web functioning and biodiversity of lake ecosystems. These results are expected to provide improved understanding of the negative effects of groundwater depletion on lake ecosystems and help management efforts.

Acknowledgments

This research was supported by grants from the National Science Foundation, CyberSEES program (award # 1331852) and Division of Environmental Biology (awards # DEB 0845932 and 1754250). This is Kellogg Biological Station contribution # 2282.

Data Availability Statement

The model used in this work (FVCOM) is an open-source community model and can be obtained from http://fvcom.smast.umassd.edu/fvcom/. All data used in this manuscript

This article is protected by copyright. All rights reserved.

have been deposited at HydroShare, CUAHSI (Safaie et al., 2021) and can be accessed using the link: https://doi.org/10.4211/hs.53b58d3a2fd24031bc0d8af3a9c4a531

References

Ambrose, R. B., Wool, T. A., & Martin, J. L. (1993). *The Water Quality Analysis Simulation Program, WASP5, Part A: Model Documentation* (pp. 1–210). Athens, Georgia: Environmental Research Laboratory, U.S. Environmental Protection Agency. Retrieved from http://journals.ametsoc.org/doi/abs/10.1175/1520-0493(2001)129%3C0569:CAALSH%3E2.0.CO;2

Anderson, E. J., Stow, C. A., Gronewold, A. D., Mason, L. A., McCormick, M. J., Qian, S. S., et al. (2021). Seasonal overturn and stratification changes drive deep-water warming in one of Earth's largest lakes. *Nature Communications*, *12*(1), 1688. https://doi.org/10.1038/s41467-021-21971-1

APHA. (1998). *Standard methods for the examination of water and wastewater* (20th ed.). Washington, DC: American Public Health Association.

ASTM D888. (2012). *Standard Test Methods for Dissolved Oxygen in Water* (No. ASTM D888-12e1). West Conshohocken, PA: ASTM International.

Blais, J. M., Schindler, D. W., Muir, D. C. G., Sharp, M., Donald, D., Lafrenière, M., et al. (2001). Melting Glaciers: A Major Source of Persistent Organochlorines to Subalpine Bow Lake in Banff National Park, Canada. *Ambio*, *30*(7), 410–415. Retrieved from https://www.jstor.org/stable/4315176

Bruesewitz, D. A., Tank, J. L., & Hamilton, S. K. (2012). Incorporating spatial variation of nitrification and denitrification rates into whole-lake nitrogen dynamics. *Journal of Geophysical Research: Biogeosciences*, *117*(G3), 543–572. https://doi.org/10.1029/2012JG002006

Brunner, P., Simmons, C. T., & Cook, P. G. (2009). Spatial and temporal aspects of the transition from connection to disconnection between rivers, lakes and groundwater. *Journal of Hydrology*, *376*(1–2), 159–169. https://doi.org/10.1016/j.jhydrol.2009.07.023

Burchard, H., Petersen, O., & Rippeth, T. P. (1998). Comparing the performance of the Mellor-Yamada and the κ-ε two-equation turbulence models. *Journal of Geophysical Research: Oceans*, *103*(C5), 10543–10554. https://doi.org/10.1029/98JC00261

Carlson, R. E. (1977). A trophic state index for lakes: Trophic state index. *Limnology and Oceanography*, *22*(2), 361–369. https://doi.org/10.4319/lo.1977.22.2.0361

Carpenter, S. R., Stanley, E. H., & Vander Zanden, M. J. (2011). State of the World's Freshwater Ecosystems: Physical, Chemical, and Biological Changes. *Annual Review of Environment and Resources*, *36*(1), 75–99. https://doi.org/10.1146/annurev-environ-021810-094524

Chang, C.-H., Cai, L.-Y., Lin, T.-F., Chung, C.-L., van der Linden, L., & Burch, M. (2015). Assessment of the Impacts of Climate Change on the Water Quality of a Small Deep Reservoir in a Humid-Subtropical Climatic Region. *Water*, *7*(4), 1687–1711. https://doi.org/10.3390/w7041687

This article is protected by copyright. All rights reserved.

Accepted Article

Chen, C., Liu, H., & Beardsley, R. C. (2003). An unstructured grid, finite-volume, three-dimensional, primitive equations ocean model: application to coastal ocean and estuaries. *Journal of Atmospheric and Oceanic Technology*, *20*(1), 159–186. Retrieved from http://journals.ametsoc.org/doi/abs/10.1175/1520-0426(2003)020%3C0159:AUGFVT%3E2.0.CO%3B2

Chen, C., Beardsley, R., & Cowles, G. (2006). An Unstructured Grid, Finite-Volume Coastal Ocean Model (FVCOM) System. *Oceanography*, *19*(1), 78–89. https://doi.org/10.5670/oceanog.2006.92

Combes, S. (2003). Protecting freshwater ecosystems in the face of global climate change. *Buying Time: A User's Manual for Building Resistance and Resilience to Climate Change in Natural Systems. WWF Climate Change Program*. Retrieved from http://climatechange.lta.org/wp-content/uploads/cct/2015/02/Protecting-freshwater-ecosystems.pdf

Comte, L., Buisson, L., Daufresne, M., & Grenouillet, G. (2013). Climate-induced changes in the distribution of freshwater fish: observed and predicted trends: *Climate change and freshwater fish*. *Freshwater Biology*, *58*(4), 625–639. https://doi.org/10.1111/fwb.12081

Covar, A. P. (1976). Selecting the Proper Reaeration Coefficient for Use in Water Quality Models. In *Proceedings of the EPA Conference on Environmental Modeling and Simulation*. Cincinnati, Ohio.

Crumpton, W. G., Isenhart, T. M., & Mitchell, P. D. (1992). Nitrate and organic N analyses with second-derivative spectroscopy. *Limnology and Oceanography*, *37*(4), 907. Retrieved from http://lib.dr.iastate.edu/bot_pubs/6/

Dalin, C., Wada, Y., Kastner, T., & Puma, M. J. (2017). Groundwater depletion embedded in international food trade. *Nature*, *543*(7647), 700–704. https://doi.org/10.1038/nature21403

Elston, R., & Wood, G. S. L. (1983). Pathogenesis of vibriosis in cultured juvenile red abalone, Haliotis rufescens Swainson. *Journal of Fish Diseases*, *6*(2), 111–128. https://doi.org/10.1111/j.1365-2761.1983.tb00059.x

Essaid, H. I., Kuwabara, J. S., Corson-Dosch, N. T., Carter, J. L., & Topping, B. R. (2020). Evaluating the dynamics of groundwater, lakebed transport, nutrient inflow and algal blooms in Upper Klamath Lake, Oregon, USA. *Science of The Total Environment*, 142768. https://doi.org/10.1016/j.scitotenv.2020.142768

Goto, D., Lindelof, K., Fanslow, D., Ludsin, S., Pothoven, S., Roberts, J., et al. (2012). Indirect consequences of hypolimnetic hypoxia on zooplankton growth in a large eutrophic lake. *Aquatic Biology*, *16*(3), 217–227. https://doi.org/10.3354/ab00442

Gurdak, J. J. (2017). Climate-induced pumping. *Nature Geoscience*, *10*(2), 71–71. https://doi.org/10.1038/ngeo2885

Gurrieri, J. T., & Furniss, G. (2004). Estimation of groundwater exchange in alpine lakes using non-steady mass-balance methods. *Journal of Hydrology*, *297*(1–4), 187–208. https://doi.org/10.1016/j.jhydrol.2004.04.021

Harris, J. O., Burke, C. M., Edwards, S. J., & Johns, D. R. (2005). Effects of oxygen supersaturation and temperature on juvenile greenlip, Haliotis laevigata Donovan, and blacklip, Haliotis rubra Leach, abalone. *Aquaculture Research*, *36*(14), 1400–1407. https://doi.org/10.1111/j.1365-2109.2005.01360.x

This article is protected by copyright. All rights reserved.

Accepted Article

Hecky, R. E., Campbell, P., & Hendzel, L. L. (1993). The stoichiometry of carbon, nitrogen, and phosphorus in particulate matter of lakes and oceans. *Limnology and Oceanography*, *38*(4), 709–724. https://doi.org/10.4319/lo.1993.38.4.0709

Ho, J. C., Michalak, A. M., & Pahlevan, N. (2019). Widespread global increase in intense lake phytoplankton blooms since the 1980s. *Nature*, *574*(7780), 667–670. https://doi.org/10.1038/s41586-019-1648-7

Jiang, L., & Fang, X. (2016). Simulation and Validation of Cisco Lethal Conditions in Minnesota Lakes under Past and Future Climate Scenarios Using Constant Survival Limits. *Water*, *8*(7), 279. https://doi.org/10.3390/w8070279

Kettle, A. J., Hughes, C., Unazi, G. A., Birch, L., Mohie-El-Din, H., & Jones, M. R. (2012). Role of groundwater exchange on the energy budget and seasonal stratification of a shallow temperate lake. *Journal of Hydrology*, *470–471*, 12–27. https://doi.org/10.1016/j.jhydrol.2012.07.004

Kinsman-Costello, L. E., O'Brien, J. M., & Hamilton, S. K. (2015). Natural stressors in uncontaminated sediments of shallow freshwaters: The prevalence of sulfide, ammonia, and reduced iron: Sulfide, ammonia, and iron in shallow freshwater sediments. *Environmental Toxicology and Chemistry*, *34*(3), 467–479. https://doi.org/10.1002/etc.2801

Kraemer, B. M., Mehner, T., & Adrian, R. (2017). Reconciling the opposing effects of warming on phytoplankton biomass in 188 large lakes. *Scientific Reports*, *7*(1), 10762. https://doi.org/10.1038/s41598-017-11167-3

Maberly, S. C., O'Donnell, R. A., Woolway, R. I., Cutler, M. E. J., Gong, M., Jones, I. D., et al. (2020). Global lake thermal regions shift under climate change. *Nature Communications*, *11*(1). https://doi.org/10.1038/s41467-020-15108-z

Magnuson, J. J. (2000). Historical Trends in Lake and River Ice Cover in the Northern Hemisphere. *Science*, *289*(5485), 1743–1746. https://doi.org/10.1126/science.289.5485.1743

O'Connor, D. J. (1983). Wind Effects on Gas- Liquid Transfer Coefficients. *Journal of Environmental Engineering*, *109*(3), 731–752. https://doi.org/10.1061/(ASCE)0733-9372(1983)109:3(731)

OECD. (1982). *Eutrophication of waters: monitoring, assessment and control*. Paris: Organisation for Economic Co-operation and Development.

O'Reilly, C. M., Alin, S. R., Plisnier, P.-D., Cohen, A. S., & McKee, B. A. (2003). Climate change decreases aquatic ecosystem productivity of Lake Tanganyika, Africa. *Nature*, *424*(6950), 766–768. https://doi.org/10.1038/nature01833

O'Reilly, C. M., Sharma, S., Gray, D. K., Hampton, S. E., Read, J. S., Rowley, R. J., et al. (2015). Rapid and highly variable warming of lake surface waters around the globe. *Geophysical Research Letters*, *42*(24), 10,773-10,781. https://doi.org/10.1002/2015GL066235

Perry, L., & Brown, C. J. D. (1942). *A fisheries survey of Gull Lake, Kalamazoo and Barry counties* (Fisheries Research Report No. 725) (pp. 1–14). Ann Arbor, Michigan, USA.: Michigan Department of Natural Resources, Fisheries Division.

Piccolroaz, S., Woolway, R. I., & Merchant, C. J. (2020). Global reconstruction of twentieth century lake surface water temperature reveals different warming trends depending on the

This article is protected by copyright. All rights reserved.

Accepted Article

climatic zone. *Climatic Change*, *160*(3), 427–442. https://doi.org/10.1007/s10584-020-02663-z

Pilla, R. M., Williamson, C. E., Zhang, J., Smyth, R. L., Lenters, J. D., Brentrup, J. A., et al. (2018). Browning- Related Decreases in Water Transparency Lead to Long- Term Increases in Surface Water Temperature and Thermal Stratification in Two Small Lakes. *Journal of Geophysical Research: Biogeosciences*, *123*(5), 1651–1665. https://doi.org/10.1029/2017JG004321

Pilla, R. M., Williamson, C. E., Adamovich, B. V., Adrian, R., Anneville, O., Chandra, S., et al. (2020). Deeper waters are changing less consistently than surface waters in a global analysis of 102 lakes. *Scientific Reports*, *10*(1), 20514. https://doi.org/10.1038/s41598-020-76873-x

Qiu, H., Hamilton, S.K. and Phanikumar, M.S. (2020). Modeling the effects of vegetation on stream temperature dynamics in a large, mixed land cover watershed in the Great Lakes region, *Journal of Hydrology*, 581, Article: 124283, pp. 1-13, doi: https://doi.org/10.1016/j.jhydrol.2019.124283.

Qiu, H., Blaen, P., Comer- Warner, S., Hannah, D. M., Krause, S., & Phanikumar, M. S. (2019). Evaluating a Coupled Phenology- Surface Energy Balance Model to Understand Stream- Subsurface Temperature Dynamics in a Mixed- Use Farmland Catchment. *Water Resources Research*, *55*(2), 1675–1697. https://doi.org/10.1029/2018WR023644

Rodell, M., Velicogna, I., & Famiglietti, J. S. (2009). Satellite-based estimates of groundwater depletion in India. *Nature*, *460*(7258), 999–1002. https://doi.org/10.1038/nature08238

Rodi, W. (1987). Examples of calculation methods for flow and mixing in stratified fluids. *Journal of Geophysical Research: Oceans*, *92*(C5), 5305–5328. Retrieved from http://onlinelibrary.wiley.com/doi/10.1029/JC092iC05p05305/fullSafaie, A. (2017). *Evaluating the Role of Groundwater in Circulation, Thermal Structure, and Nutrient-Algal Dynamics within a Deep Inland Lake*,Ph.D. Dissertation, Department of Civil & Environmental Engineering, Michigan State University, East Lansing, Michigan, United States.

Safaie, A., Litchman, E., & Phanikumar, M.S. (2021). Gull Lake Field Data 2014-15, HydroShare, https://doi.org/10.4211/hs.53b58d3a2fd24031bc0d8af3a9c4a531

Safaie, A., Litchman, E., & Phanikumar, M. S. (2017a). Evaluating the role of groundwater on circulation and thermal structure in a deep, inland lake. *Advances in Water Resources*, vol. 108, pp. 310-327, doi: 10.1016/j.advwatres.2017.08.002

Safaie, A., Dang, C., Qiu, H., Radha, H., & Phanikumar, M. S. (2017b). Manifold methods for assimilating geophysical and meteorological data in Earth system models and their components. *Journal of Hydrology*, *544*, 383–396. https://doi.org/10.1016/j.jhydrol.2016.11.009

Schladow, S. G., & Hamilton, D. P. (1997). Prediction of water quality in lakes and reservoirs: Part II - Model calibration, sensitivity analysis and application. *Ecological Modelling*, *96*(1–3), 111–123. https://doi.org/10.1016/S0304-3800(96)00063-4

Schneider, P., & Hook, S. J. (2010). Space observations of inland water bodies show rapid surface warming since 1985. *Geophysical Research Letters*, *37*(22), 1–5. https://doi.org/10.1029/2010GL045059

This article is protected by copyright. All rights reserved.

Accepted Article

Sharma, S., Gray, D. K., Read, J. S., O'Reilly, C. M., Schneider, P., Qudrat, A., et al. (2015). A global database of lake surface temperatures collected by in situ and satellite methods from 1985–2009. *Scientific Data*, *2*, 150008. https://doi.org/10.1038/sdata.2015.8

Sharma, S., Blagrave, K., Magnuson, J. J., O'Reilly, C. M., Oliver, S., Batt, R. D., et al. (2019). Widespread loss of lake ice around the Northern Hemisphere in a warming world. *Nature Climate Change*, *9*(3), 227–231. https://doi.org/10.1038/s41558-018-0393-5

Shaw, G. D., Mitchell, K. L., & Gammons, C. H. (2017). Estimating groundwater inflow and leakage outflow for an intermontane lake with a structurally complex geology: Georgetown Lake in Montana, USA. *Hydrogeology Journal*, *25*(1), 135–149. https://doi.org/10.1007/s10040-016-1500-1

Shigesada, N., & Okubo, A. (1981). Analysis of the self-shading effect on algal vertical distribution in natural waters. *Journal of Mathematical Biology*, *12*(3), 311–326. Retrieved from http://www.springerlink.com/index/k3056t3066656635.pdf

Skaskevych, A., Lee, J., Jung, H. C., Bolten, J., David, J. L., Policelli, F. S., et al. (2020). Application of GRACE to the estimation of groundwater storage change in a data- poor region: A case study of Ngadda catchment in the Lake Chad Basin. *Hydrological Processes*, *34*(4), 941–955. https://doi.org/10.1002/hyp.13613

Smagorinsky, J. (1963). General circulation experiments with the primitive equations: I. The basic experiment. *Monthly Weather Review*, *91*(3), 99–164. https://doi.org/10.1175/1520-0493(1963)091<0099:GCEWTP>2.3.CO;2

Steele, J. H. (1962). Environmental control of photosynthesis in the sea. *Limnology and Oceanography*, *7*(2), 137–150. https://doi.org/10.4319/lo.1962.7.2.0137

Tague, D. F. (1977). *The hydrologic and total phosphorus budgets of Gull Lake, Michigan*. Michigan State University, East Lansing, Michigan, United States.

Tanentzap, A. J., Morabito, G., Volta, P., Rogora, M., Yan, N. D., & Manca, M. (2020). Climate warming restructures an aquatic food web over 28 years. *Global Change Biology*, *26*(12), 6852–6866. https://doi.org/10.1111/gcb.15347

Timoshkin, O. A., Moore, M. V., Kulikova, N. N., Tomberg, I. V., Malnik, V. V., Shimaraev, M. N., et al. (2018). Groundwater contamination by sewage causes benthic algal outbreaks in the littoral zone of Lake Baikal (East Siberia). *Journal of Great Lakes Research*, *44*(2), 230–244. https://doi.org/10.1016/j.jglr.2018.01.008

Tong, Y., Xiwen, X., Miao, Q., Jingjing, S., Yiyan, Z., Wei, Z., et al. (2021). Lake warming intensifies the seasonal pattern of internal nutrient cycling in the eutrophic lake and potential impacts on algal blooms. *Water Research*, *188*, 116570. https://doi.org/10.1016/j.watres.2020.116570

Turner, J. V., & Townley, L. R. (2006). Determination of groundwater flow-through regimes of shallow lakes and wetlands from numerical analysis of stable isotope and chloride tracer distribution patterns. *Journal of Hydrology*, *320*(3–4), 451–483. https://doi.org/10.1016/j.jhydrol.2005.07.050

Umaña, G. (2014). Ten years of limnological monitoring of a modified natural lake in the tropics: Cote Lake, Costa Rica. *Revista de Biología Tropical*, *62*(2), 576–578. Retrieved from http://www.scielo.sa.cr/scielo.php?pid=S0034-77442014000100013&script=sci_arttext&tlng=en

This article is protected by copyright. All rights reserved.

Accepted Article

Verburg, P. (2003). Ecological Consequences of a Century of Warming in Lake Tanganyika. *Science*, *301*(5632), 505–507. https://doi.org/10.1126/science.1084846

Wada, Y., van Beek, L. P. H., van Kempen, C. M., Reckman, J. W. T. M., Vasak, S., & Bierkens, M. F. P. (2010). Global depletion of groundwater resources. *Geophysical Research Letters*, *37*(20), 1–5. https://doi.org/10.1029/2010GL044571

Wang, W. (2018). Global lake evaporation accelerated by changes in surface energy allocation in a warmer climate. *Nature Geoscience*, 7.

Webster, K. E., Kratz, T. K., Bowser, C. J., Magnuson, J. J., & Rose, W. J. (1996). The influence of landscape position on lake chemical responses to drought in northern Wisconsin. *Limnology and Oceanography*, *41*(5), 977–984. Retrieved from http://www.acad.carleton.edu/curricular/BIOL/classes/bio252/Websteretal96LO.pdf

Winslow, L. A., Read, J. S., Hansen, G. J. A., & Hanson, P. C. (2015). Small lakes show muted climate change signal in deepwater temperatures. *Geophysical Research Letters*, *42*(2), 2014GL062325. https://doi.org/10.1002/2014GL062325

Woolway, R. I., & Maberly, S. C. (2020). Climate velocity in inland standing waters. *Nature Climate Change*, *10*(12), 1124–1129. https://doi.org/10.1038/s41558-020-0889-7

Woolway, R. I., & Merchant, C. J. (2018). Intralake Heterogeneity of Thermal Responses to Climate Change: A Study of Large Northern Hemisphere Lakes. *Journal of Geophysical Research: Atmospheres*, *123*(6), 3087–3098. https://doi.org/10.1002/2017JD027661

Woolway, R. I., Jones, I. D., Maberly, S. C., French, J. R., Livingstone, D. M., Monteith, D. T., et al. (2016). Diel surface temperature range scales with lake size. *PloS One*, *11*(3), e0152466. Retrieved from http://journals.plos.org/plosone/article?id=10.1371/journal.pone.0152466

Woolway, R. I., Kraemer, B. M., Lenters, J. D., Merchant, C. J., O'Reilly, C. M., & Sharma, S. (2020). Global lake responses to climate change. *Nature Reviews Earth & Environment*, *1*(8), 388–403. https://doi.org/10.1038/s43017-020-0067-5

Xiao, X., Agustí, S., Pan, Y., Yu, Y., Li, K., Wu, J., & Duarte, C. M. (2019). Warming Amplifies the Frequency of Harmful Algal Blooms with Eutrophication in Chinese Coastal Waters. *Environmental Science & Technology*, *53*(22), 13031–13041. https://doi.org/10.1021/acs.est.9b03726

Yacobi, Y. Z., & Zohary, T. (2010). Carbon:chlorophyll a ratio, assimilation numbers and turnover times of Lake Kinneret phytoplankton. *Hydrobiologia*, *639*(1), 185–196. https://doi.org/10.1007/s10750-009-0023-3

Yassuda, E. A., Davie, S. R., Mendelsohn, D. L., Isaji, T., & Peene, S. J. (2000). Development of a waste load allocation model for the Charleston Harbor estuary, phase II: water quality. *Estuarine, Coastal and Shelf Science*, *50*(1), 99–107. Retrieved from http://www.sciencedirect.com/science/article/pii/S027277149990536X

Zhang, Y., Su, Y., Liu, Z., Jeppesen, E., Yu, J., & Jin, M. (2016). Geochemical records of anoxic water mass expansion in an oligotrophic alpine lake (Yunnan Province, SW China) in response to climate warming since the 1980s. *The Holocene*, 0959683616645948. Retrieved from http://hol.sagepub.com/content/early/2016/05/11/0959683616645948.abstract

Zhang, Y., Wu, Z., Liu, M., He, J., Shi, K., Zhou, Y., et al. (2015). Dissolved oxygen stratification and response to thermal structure and long-term climate change in a large and

This article is protected by copyright. All rights reserved.

deep subtropical reservoir (Lake Qiandaohu, China). *Water Research*, *75*, 249–258. https://doi.org/10.1016/j.watres.2015.02.052

Zheng, L., Chen, C., & Zhang, F. Y. (2004). Development of water quality model in the Satilla River Estuary, Georgia. *Ecological Modelling*, *178*(3–4), 457–482. https://doi.org/10.1016/j.ecolmodel.2004.01.016

Accepted Article

This article is protected by copyright. All rights reserved.

Accepted Article

Figures and Tables

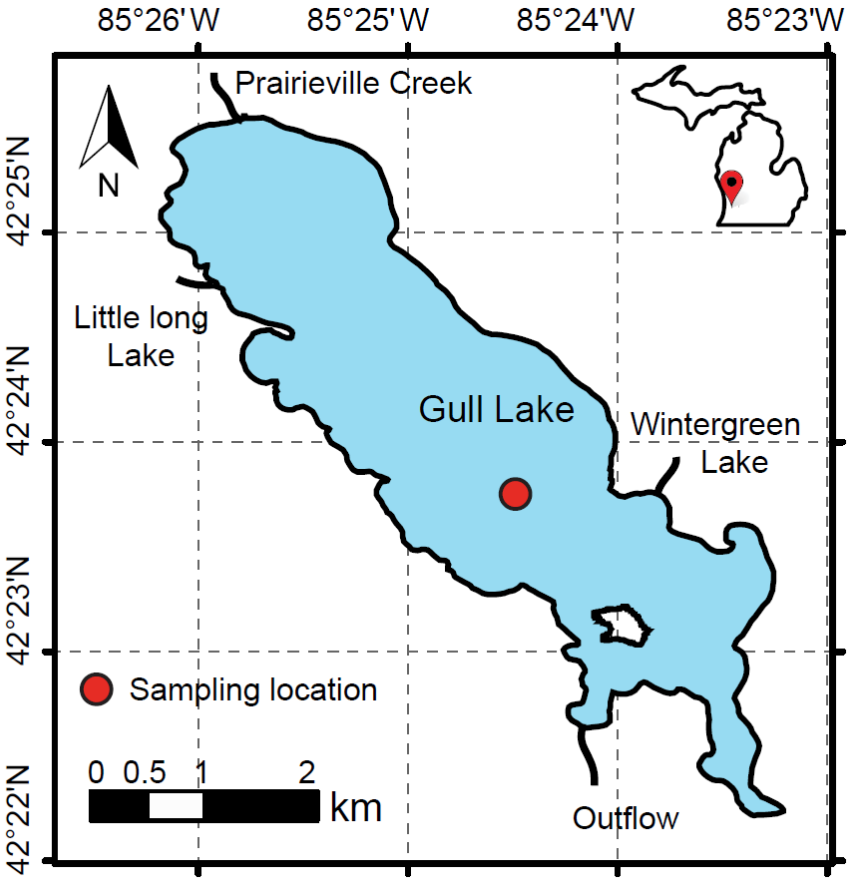

Figure 1. Map of Gull Lake, MI showing the sampling location of water quality parameters.

This article is protected by copyright. All rights reserved.

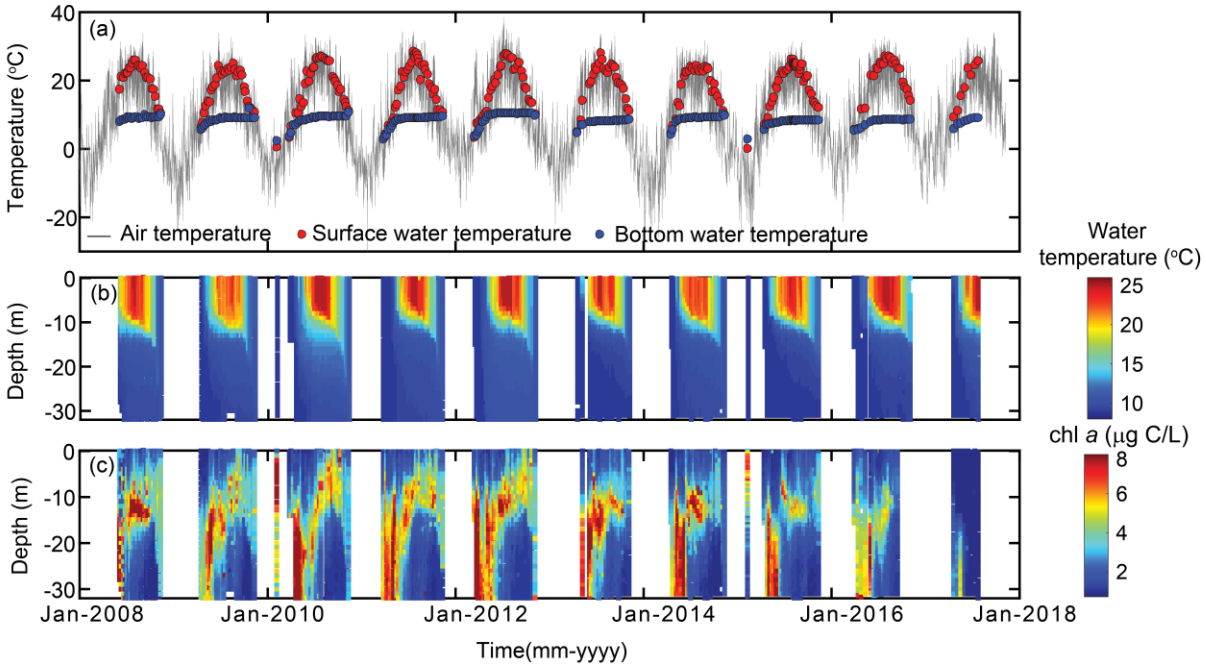

Figure 2. (a) Time series of bottom water temperature (blue symbols) measured at a depth of 32 m compared to the surface water temperature (red symbols) and air temperature (gray line). (b) contour plot of measured water temperature (°C), (c) contour plot of observed chl-*a* (μg C/L) between 2008 and 2017.

This article is protected by copyright. All rights reserved.

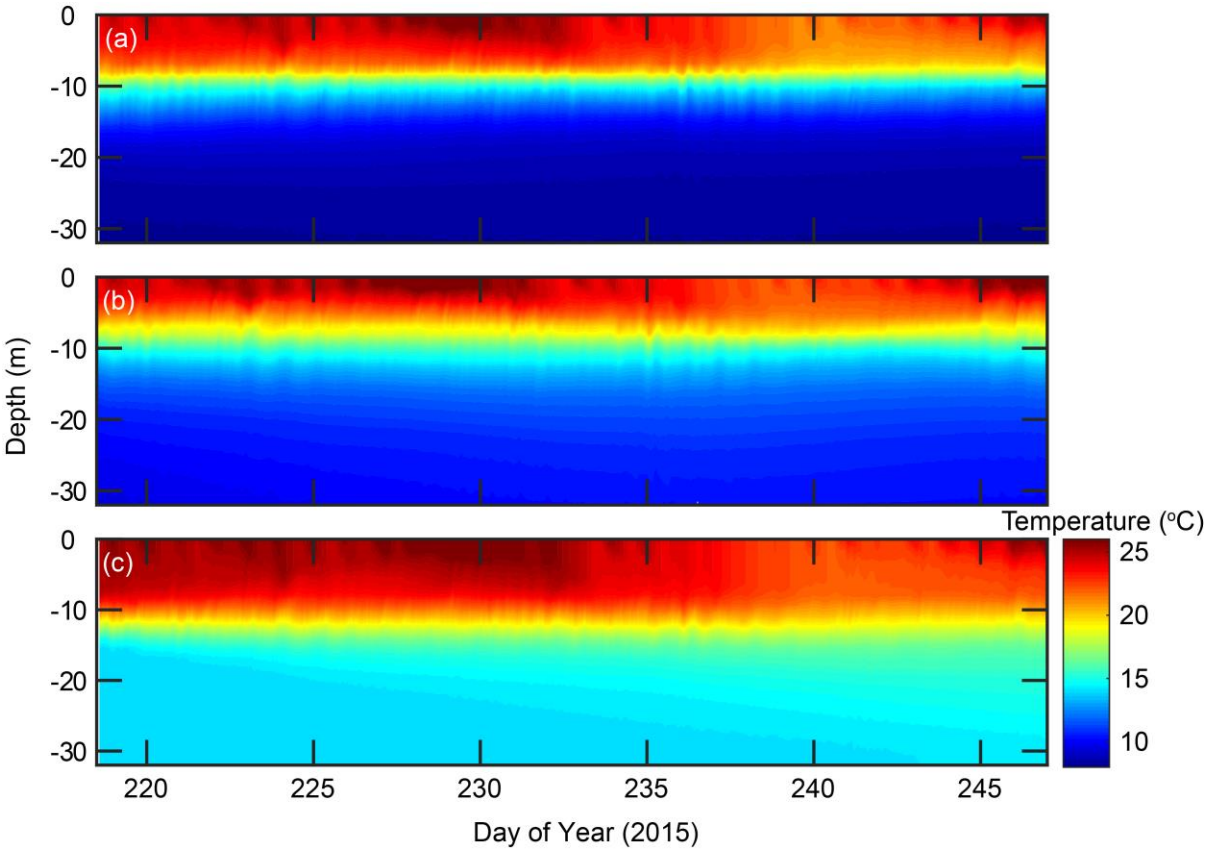

Figure 3. Contour plots of simulated water temperature (°C) for Gull Lake in 2015 (a) with full groundwater contribution reflecting current conditions (scenario 1) (b) with half of the current contribution of groundwater (scenario 2) and (c) in the absence of any groundwater contribution to the lake (scenario 3).

Accepted Article

This article is protected by copyright. All rights reserved.

Accepted Article

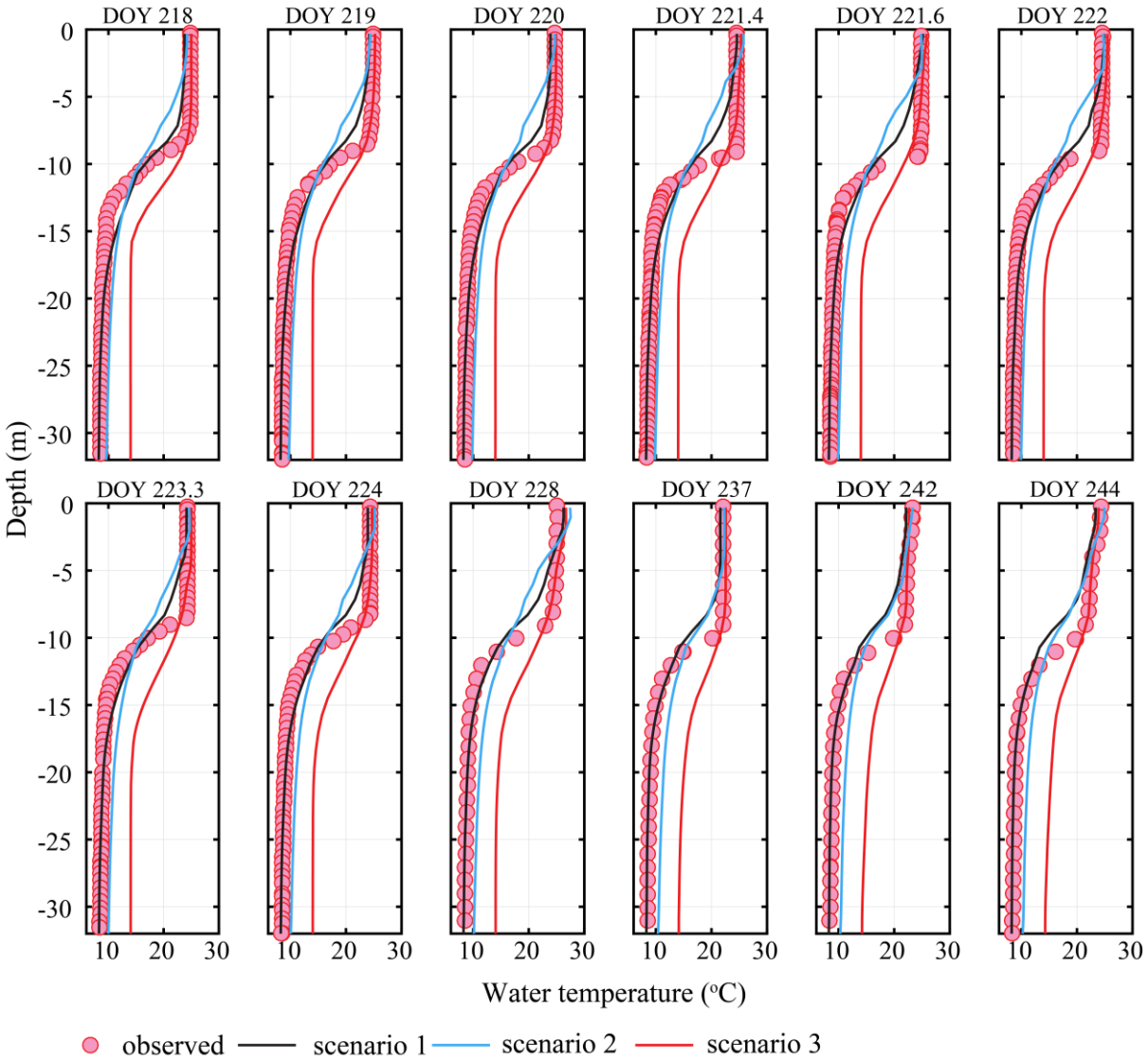

Figure 4. Comparisons of simulated vertical profiles of water temperature (°C) with observed data in 2015. Simulated results of scenario1 (black line) reflect current conditions with full groundwater contribution, results of scenario 2 (blue line) are with half of the current groundwater contribution to the lake and results of scenario 3 (red line) are in the absence of any groundwater contribution to the lake.

This article is protected by copyright. All rights reserved.

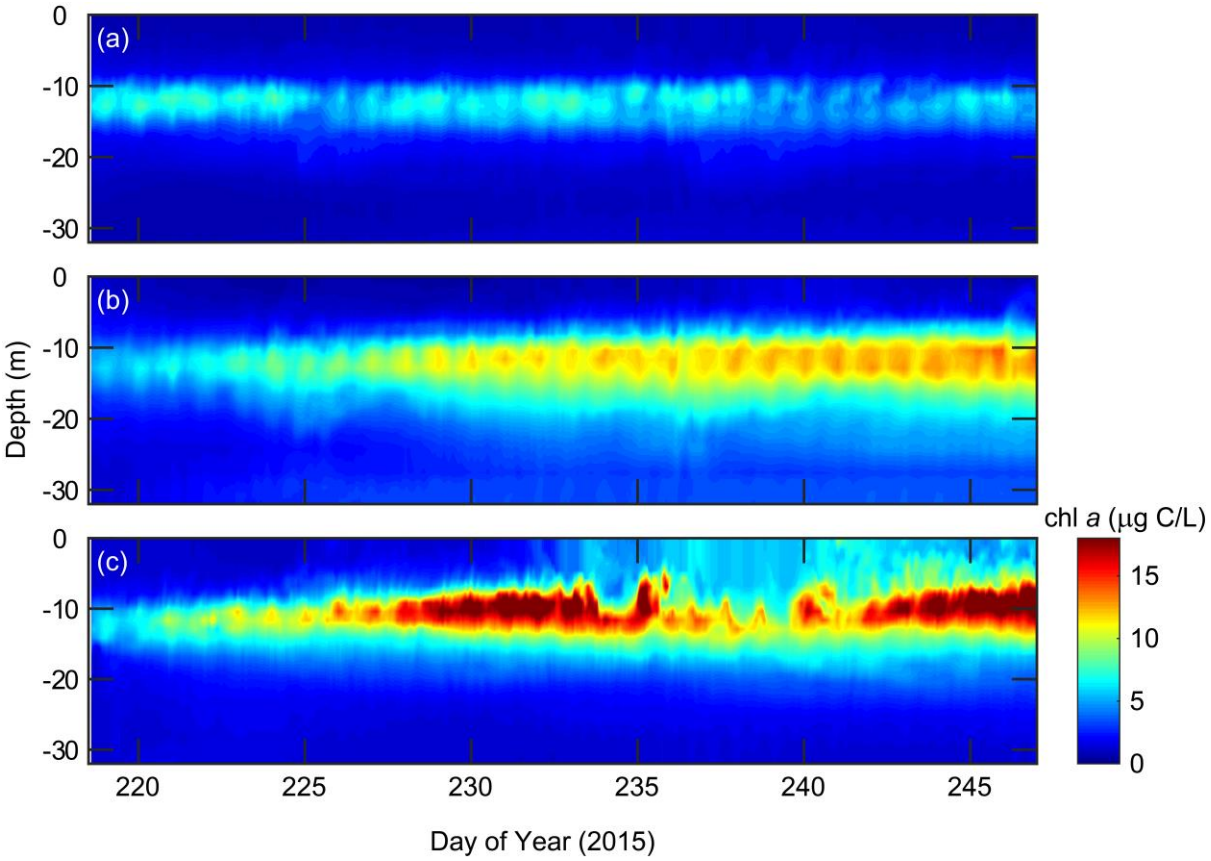

Figure 5. Contour plots of simulated chl *a* (μg C/L) for Gull Lake in 2015 (a) with full groundwater contribution reflecting current conditions (scenario 1) (b) with half of the current contribution of groundwater (scenario 2) and (c) in the absence of any groundwater contribution to the lake (scenario 3).

Accepted Article

This article is protected by copyright. All rights reserved.

Accepted Article

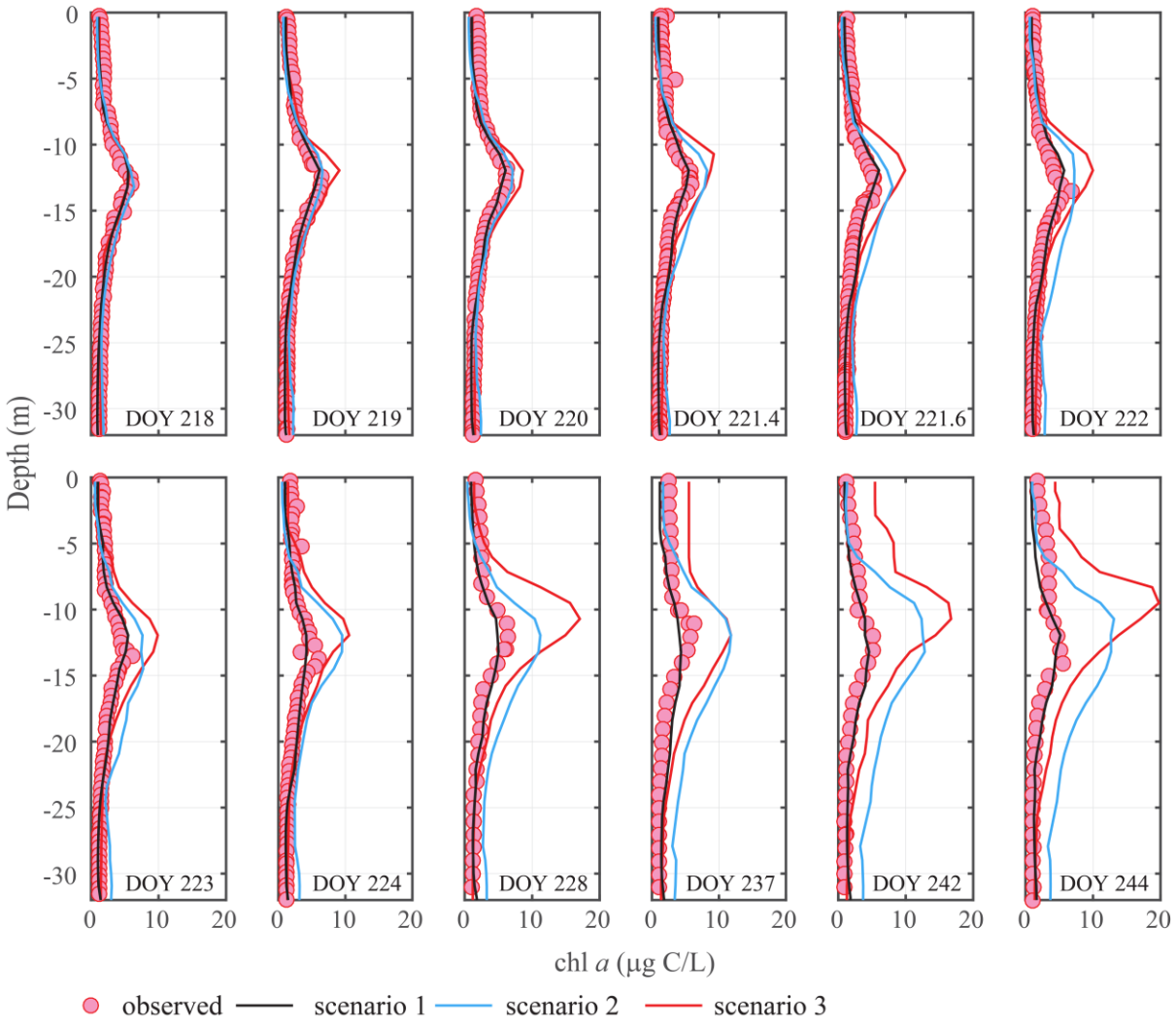

Figure 6. Comparisons of simulated vertical profiles of chl-*a* (µg C/L) with observed data in 2015. Simulated results of scenario 1 (black line) reflect current groundwater contribution to the lake, results of scenario 2 (blue line) are with half of the current groundwater contribution and results of scenario 3 (red line) are in the absence of any groundwater contribution to the lake.

This article is protected by copyright. All rights reserved.

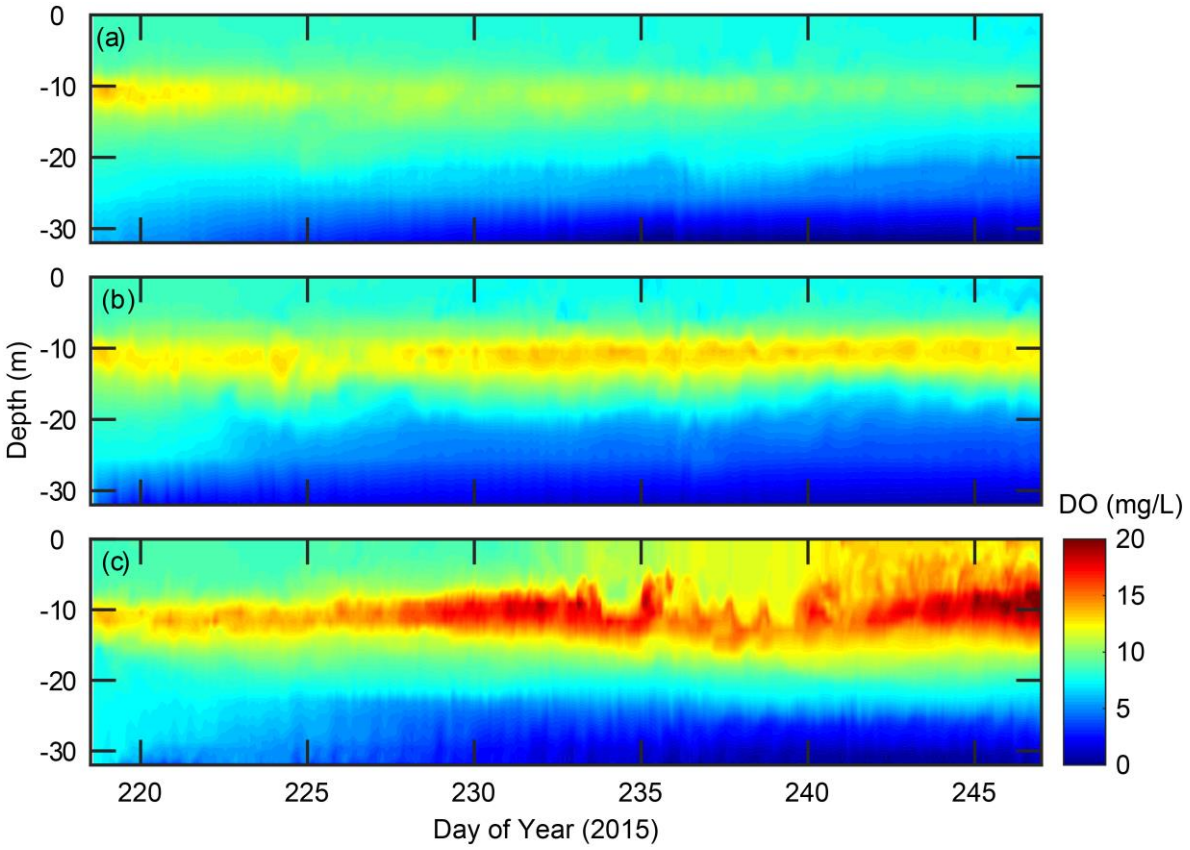

Figure 7. Contour plots of simulated DO (mg O_2/L) (a) with current groundwater contribution to the lake (scenario 1) (b) with half of the current groundwater contribution (scenario 2) and (c) in the absence of any groundwater contribution (scenario 3) for Gull Lake in 2015.

Accepted Article

This article is protected by copyright. All rights reserved.

Accepted Article

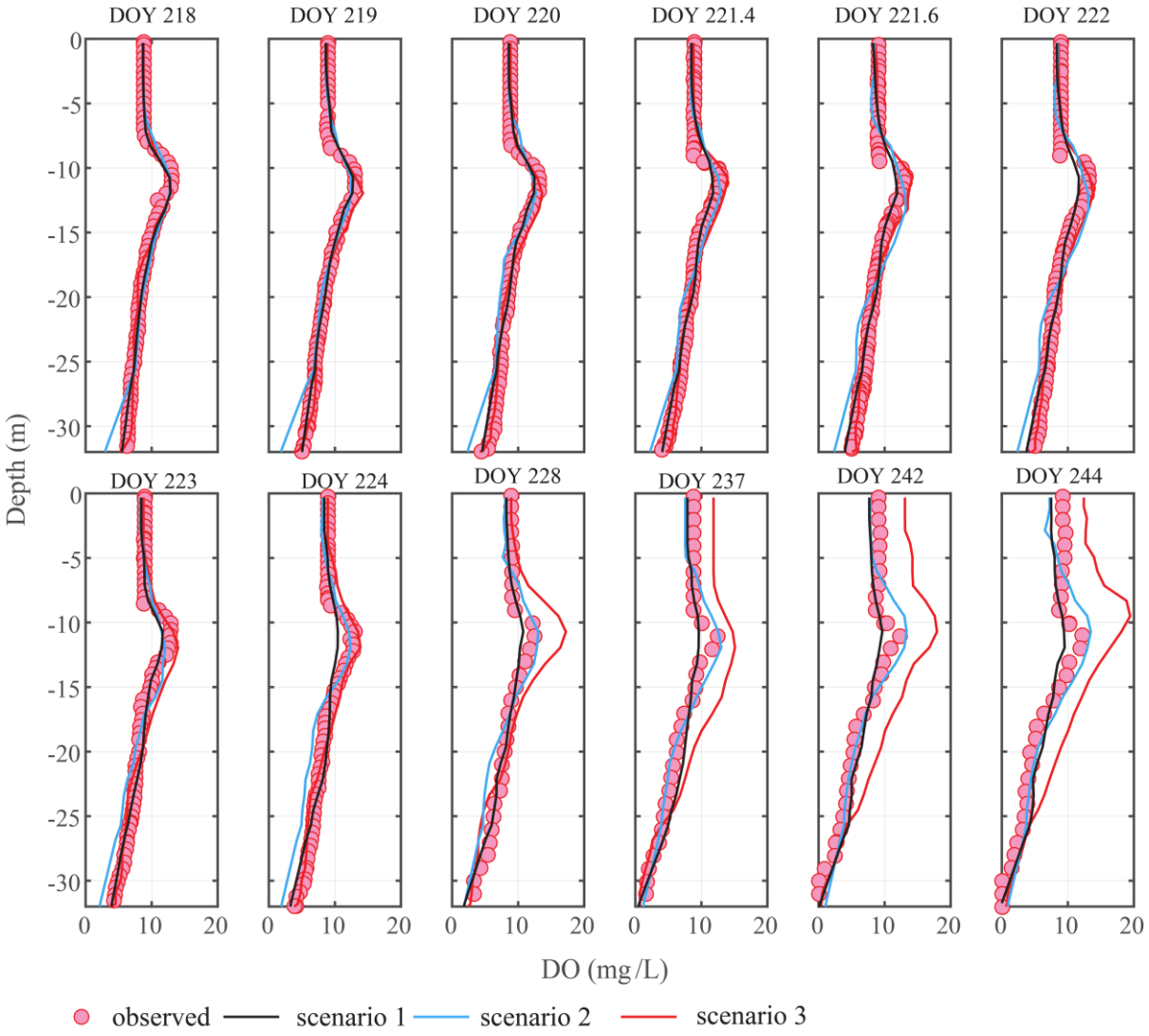

Figure 8. Comparisons of simulated vertical profiles of dissolved oxygen (mg O_2/L) with observed data in 2015. Simulated results of scenario 1 (black line) reflect current groundwater contribution to the lake, results of scenario 2 (blue line) are with half of the current groundwater contribution and results of scenario 3 (red line) are in the absence of any groundwater contribution to the lake.

This article is protected by copyright. All rights reserved.

Accepted Article

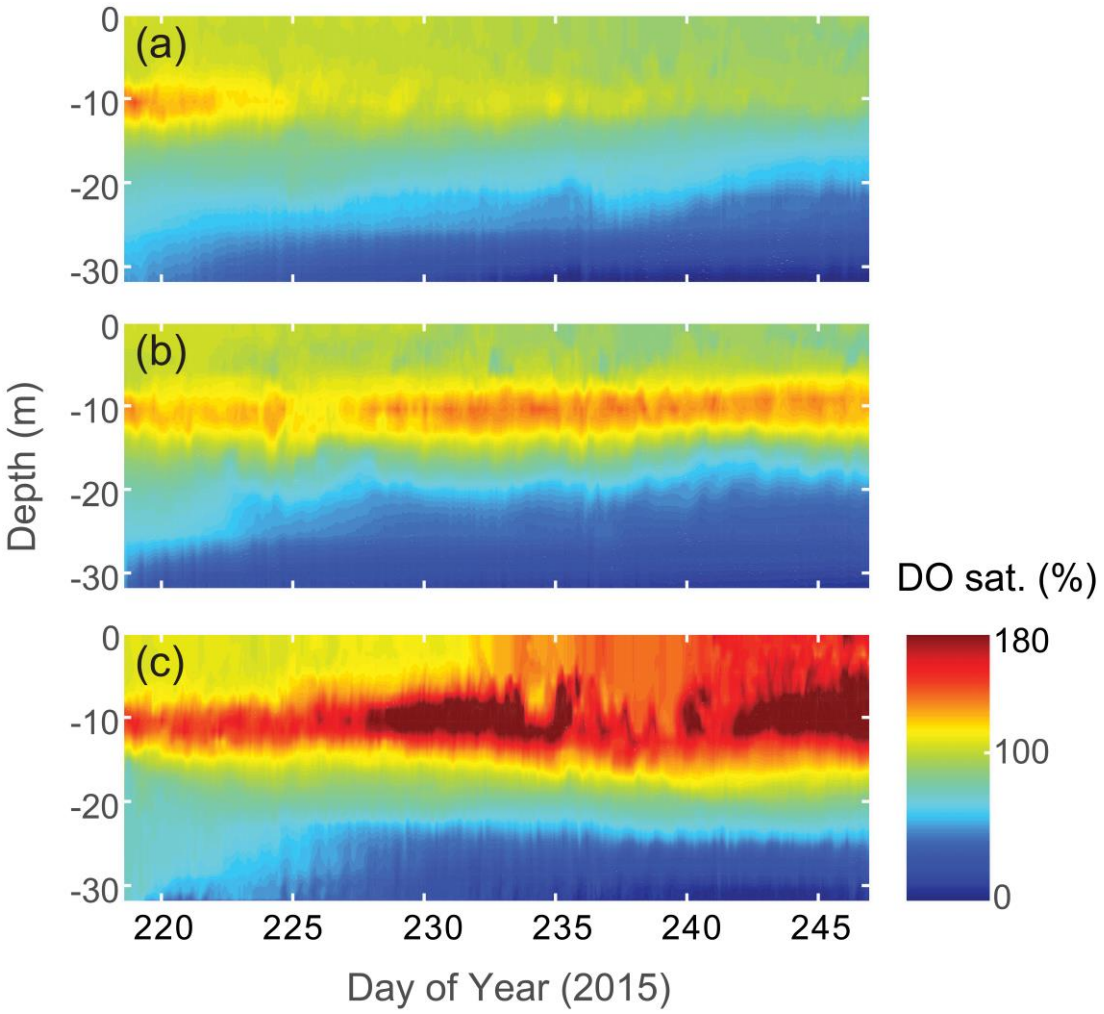

Figure 9. Contour plots of simulated DO saturation (%), (a) with current groundwater contribution to the lake (scenario 1) (b) with half of the current groundwater contribution (scenario 2) and (c) in the absence of any groundwater contribution (scenario 3) for Gull Lake in 2015.

This article is protected by copyright. All rights reserved.

Accepted Article

Table 1. Information of the nutrient concentrations observed in Prairieville Creek and the pond lab reservoir well near Gull Lake from 2009-2014.

Nutrient forms	Prairieville Creek			Pond Lab Reservoir well		
	average	min	max	average	min	max
NO3 (mg/L)	5.70	4.90	6.40	0.026	0.001	0.500
NH4 (μg/L)	28.0	8.30	68.0	14.0	0.73	33.0
TDP (μg/L)	5.97	2.30	9.14	5.13	0.66	14.0
PO4 (μg/L)	1.80	0.72	3.87	4.12	0.36	14.0

This article is protected by copyright. All rights reserved.

Table 2. Water quality parameter values used in FVCOM-WQM

Symbol	Value	Definition
k_{deox}	0.05[a]	Deoxygenation rate at 20 degree (day^{-1})
k_{nitr}	0.09[a]	Nitrification rate at 20 degree (day^{-1})
k_{resp}	0.071[b]	Phytoplankton respiration rate at 20 degree (day^{-1})
k_{bresp}	0.20[c]	Bacterial respiration rate (uM/h)
k_{deni}	0.09[a]	Denitrification rate at 20 degree (day^{-1})
k_{grow}	1.21[b]	Optimum phytoplankton growth rate at 20 degree, (day^{-1})
k_{mort}	0.04[b]	Mortality rate of phytoplankton at 20 degree, (day^{-1})
k_{mine1}	0.075[b]	Organic nitrogen mineralization at 20 degree (day^{-1})
k_{mine2}	0.22[b]	Organic phosphorus mineralization at 20 degree (day^{-1})
q_{reae}	1.028[a]	Temperature coefficient of reaeration
q_{deox}	1.047[a]	Temperature coefficient of deoxygenation
q_{nitr}	1.08[a]	Temperature coefficient of nitrification
q_{resp}	1.08[a]	Temperature coefficient of phytoplankton respiration
q_{deni}	1.08[a]	Temperature coefficient of denitrification
q_{grow}	1.07[8]	Temperature coefficient of optimum growth
q_{mort}	1.00[a]	Temperature coefficient of phytoplankton mortality
q_{mine1}	1.08[a]	Temperature coefficient of nitrogen mineralization
q_{mine2}	1.08[a]	Temperature coefficient of phosphorus mineralization
q_{SOD}	1.08[a]	Temperature coefficient of SOD
SOD	2.5[a]	Sediment oxygen demand
h_b	0.5[d]	Benthic layer depth (m)
K_{BOD}	0.5[a]	Half-saturation constant for oxygen limitation of CBOD oxidation (mg O_2/l)
K_{nitr}	0.5[a]	Half-saturation constant for oxygen limitation of nitrification (mg O_2/l)
K_{mN}	25[a]	Half-saturation constant for uptake of inorganic nitrogen (μg N/l)
K_{mP}	1[a]	Half-saturation constant for uptake of inorganic phosphorus (μg P/l)
K_{NO_3}	0.1[a]	Half-saturation constant for oxygen limitation of denitrification (mg O_2/l)
K_{mPC}	1[a]	Half-saturation constant of phytoplankton limitation of phosphorus recycle (mg C/l)
D_z	0.76[*]	Diffusive exchange coefficient (m^2/day)
v_{S2}	0.5[a]	Organic matter sinking velocity (m/day)
v_{S3}	0.14[*]	Phytoplankton settling velocity (m/day)
v_{S6}	0.5[a]	Settling velocity of organic nitrogen ($m.day^{-1}$)
v_{S8}	0.5[a]	Settling velocity of organic phosphorus ($m.day^{-1}$)
f_{D2}	0.5[a]	Fraction of dissolved CBOD
f_{D6}	1[a]	Fraction of dissolved organic nitrogen
f_{D8}	1[a]	Fraction of dissolved organic phosphorus
f_{ON}	0.65[c]	Fraction of dead and respired phytoplankton recycled to the organic nitrogen pool
f_{OP}	0.65[c]	Fraction of dead and respired phytoplankton recycled to the organic phosphorus pool
a_{cchl}	60[e]	Ratio of carbon to chlorophyll
a_{nc}	1/12.5[f]	Ratio of nitrogen to carbon in phytoplankton (mg N/mg C)
a_{pc}	1/412[f]	Ratio of phosphorus to carbon in phytoplankton (mg P/mg C)

[a] (Ambrose et al., 1993) [b] (Schladow & Hamilton, 1997) [c] (Yassuda et al., 2000) [d] (Zheng et al., 2004)
[e] (Yacobi & Zohary, 2010) [f] (Hecky et al., 1993) [*] This study

This article is protected by copyright. All rights reserved.

Table 3. Model performance metrics used for evaluating the water quality model against observed data for vertical water quality profiles.

Parameter	Year	R^2	RMSE
Water temperature (^oC)	2014	0.96	0.60
	2015	0.99	0.79
Chl-a (µg C/L)	2014	0.91	0.72
	2015	0.87	0.62
Dissolved oxygen (mg O_2/L)	2014	0.96	1.32
	2015	0.96	0.77
Dissolved nitrate (mg N/L)	2014	0.68	0.13
	2015	0.95	0.09
SRP (µg P/L)	2014	0.74	0.80
	2015	0.68	0.18

Accepted Article

This article is protected by copyright. All rights reserved.

Table 4. Summary of mean and maximum simulated chlorophyll-a and the Trophic State Index (TSI) from scenarios 1-3

	2014			2015		
	Scenario1	Scenario2	Scenario3	Scenario1	Scenario2	Scenario3
Mean chl-*a* (μg/L)	2.25	2.99	3.44	2.22	4.73	4.68
Max chl-*a* (μg/L)	8.48	11.1	24.59	6.71	15.40	25.16
TSI	32.2	28.5	38.5	31.4	30.8	41.0

Accepted Article

This article is protected by copyright. All rights reserved.